Published in final edited form as:
Cancer Res. 2009 October 1; 69(19): 7721–7728. doi:10.1158/0008-5472.CAN-09-1419.

[^{18}F]Fluoromethyl-[1,2-$^{2}H_4$]-choline: A novel radiotracer for imaging choline metabolism in tumors by positron emission tomography

Julius Leyton[1], **Graham Smith**[1], **Yongjun Zhao**[2], **Meg Perumal**[1], **Quang-De Nguyen**[1], **Edward Robins**[2], **Erik Årstad**[2], and **Eric O. Aboagye**[1]

[1]Molecular Therapy Group, Faculty of Medicine, Imperial College London

[2]MDx Discovery (part of GE Healthcare) at Hammersmith Imanet Ltd., Hammersmith Hospital, Du Cane Road London W12 0NN, UK.

Abstract

Current radiotracers for positron emission tomography (PET) imaging of choline metabolism have poor systemic metabolic stability *in vivo*. We describe a novel radiotracer, [^{18}F]fluoromethyl-[1,2-$^{2}H_4$]-choline (D4-FCH), that employs deuterium isotope effect to improve metabolic stability. D4-FCH proved more resistant to oxidation than its non-deuterated analog, [^{18}F]fluoromethylcholine (FCH), in plasma, kidneys, liver and tumor, while retaining phosphorylation potential. Tumor radiotracer levels, a determinant of sensitivity in imaging studies, was improved by deuterium substitution; tumor uptake values expressed as %injected dose/voxel at 60 min were 7.43 ± 0.47 and 5.50 ± 0.49 for D4-FCH and FCH, respectively, ($P = 0.04$). D4-FCH was also found to be a useful response biomarker. Treatment with the mitogenic extracellular kinase inhibitor, PD0325901, resulted in a reduction in tumor radiotracer uptake that occurred in parallel with reductions in choline kinase A expression. In conclusion, D4-FCH is a very promising metabolically stable radiotracer for imaging choline metabolism in tumors.

Keywords

[^{18}F]Fluoromethyl-[1,2-$^{2}H_4$]-choline; positron emission tomography; imaging; choline metabolism; therapy response

Introduction

The biosynthetic product of choline kinase (EC 2.7.1.32) activity, phosphocholine, is elevated in several cancers and is a precursor for membrane phosphatidylcholine (1-4). Over-expression of choline kinase and increased enzyme activity have been reported in prostate, breast, lung, ovarian and colon cancers (5-10) and are largely responsible for the increased phosphocholine levels with malignant transformation and progression; the increased phosphocholine levels in cancer cells are also due to increased breakdown via phospholipase C (6). Because of this phenotype, together with reduced urinary excretion, [^{11}C]choline has become a prominent radiotracer for positron emission tomography (PET)

Requests for reprints: Eric O. Aboagye, Molecular Therapy Research Group, Faculty of Medicine, Imperial College London, Room 240 MRC Cyclotron Building, Hammersmith Hospital, Du Cane Road, London, W12 ONN, United Kingdom Telephone: 02083833759; Fax: 02083831783; eric.aboagye@imperial.ac.uk.

Disclosure of Potential Conflict of Interest
The authors are considering filing a patent on this invention.

Europe PMC Funders Author Manuscripts

and PET-Computed Tomography (PET-CT) imaging of prostate cancer, and to a lesser extent imaging of brain, esophageal, and lung cancer (11-16). The specific PET signal is due to transport and phosphorylation of the radiotracer to [^{11}C]phosphocholine by choline kinase. [^{18}F]Fluoromethylcholine (FCH) was developed to overcome the short physical half-life of carbon-11 (20.4 min) (17) and a number of PET and PET-CT studies with this relatively new radiotracer have been published (18-21). The longer half-life of fluorine-18 (109.8 min) was deemed potentially advantageous in permitting late imaging of tumors when sufficient clearance of parent tracer in systemic circulation had occurred (22). Of interest, however, [^{11}C]choline (and fluoro-analog) is oxidized to [^{11}C]betaine by choline oxidase (EC 1.1.3.17) mainly in kidney and liver tissues, with metabolites detectable in plasma soon after injection of the radiotracer (23). This makes discrimination of the relative contributions of parent radiotracer and catabolites difficult when a late imaging protocol is used. In this article we have developed a more metabolically stable FCH analog, [^{18}F]fluoromethyl-[1,2-$^{2}H_4$]-choline (D4-FCH), based on the deuterium isotope effect (24-27). This novel radiotracer has a number of potential advantages: (i) due to improved stability it should better enable late imaging of tumors after sufficient clearance of the radiotracer from systemic circulation and (ii) it should enhance the sensitivity of tumor imaging through increased availability of substrate. In this article, we report for the first time, the development of D4-FCH for imaging tumors and for monitoring therapeutic response.

Materials and Methods

Radiopharmaceuticals and drug

No-carrier-added FCH and D4-FCH were synthesized by reacting [^{18}F]fluorobromomethane with N, N-dimethylaminoethanol or D4-N,N-dimethylaminoethanol, respectively, as shown in Fig. 1a. [^{18}F]Fluorobromomethane was synthesized from dibromomethane by substitution of bromine with [^{18}F]fluoride based on the method reported by Bergman (28). After trapping the [^{18}F]fluorobromomethane into a 2.5ml conical glass vial containing 150μl of dimethylaminoethanol or D4-N,N-dimethylaminoethanol in dry acetonitrile (1.0ml) pre-cooled to 0°C, the vial was sealed and heated to 100°C for 10 min. The solvent was removed by a stream of nitrogen. Following this, the residue containing FCH or D4-FCH was dissolved in 5% ethanol solution (10ml), loaded onto a cation exchange Sep Pak Cartridge (Waters, Accell CM light) which had been pre-conditioned with 2M HCl and water (5ml each). After further washing of the CM cartridge with ethanol and water (10 ml each), the FCH or D4-FCH was eluted with sterile isotonic saline (0.5 to 2.0ml) and sterilized by filtration (0.22 μm sterile filter; Millipore, Waters).

The radiochemical purity for both FCH and D4-FCH was ~ 99% as analyzed with radiochemical detection (radio-HPLC). The radioactive species were confirmed as the desired choline analogs by co-elution with a commercial fluorocholine chloride standard (obtained from ABCR Gmbh & Co, Karlsruhe, Germany) by HPLC on an Agilent 1100 series HPLC system equipped with a Bioscan Flowcount FC-3400 Pin diode detector (for radioactivity detection) and an Agilent G1362A refractive index detector for detection of non-radioactive species. The stationary phase comprised of a Phenomenex Luna C_{18} reverse-phase column (150 mm × 4.6 mm) and the mobile phase comprised 5 mM heptanesulfonic acid (pH 8.0) and acetonitrile (90:10 v/v), delivered at a flow rate 1 mL/min. [^{11}C]Choline was synthesized by Hammersmith Imanet Limited using a previously described method (29). PD0325901 (*N*-((*R*)-2,3-dihydroxy-propoxy)-3,4-difluoro-2-(2-fluoro-4-iodo-phenylamino)-benzamide) was obtained from the Division of Signal Transduction Therapy, University of Dundee, Dundee, Scotland.

Animals and tumor models

All animal experiments were done by licensed investigators in accordance with the United Kingdom Home Office Guidance on the Operation of the Animal (Scientific Procedures) Act 1986 and within guidelines set out by the United Kingdom Coordinating Committee for Cancer Research's Ad hoc Committee on Welfare of Animals in Experimental Neoplasia (30). Both tumor-bearing (Balb/c nude mice) and non-tumor bearing (Balb/c mice) animals were used. Human melanoma, SKMEL-28, and human colon, HCT116, tumors were grown in Balb/c *nu/nu* mice (Harlan) as previously reported (31). Tumor dimensions were measured continuously using a caliper and tumor volumes were calculated by the equation: volume = (π/6) × a × b × c, where a, b, and c represent three orthogonal axes of the tumor. Mice were used when their tumors reached approximately 100 mm^3.

Oxidation potential of FCH and D4-FCH *in vivo.*

FCH or D4-FCH (~4.8MBq) was injected via the tail vein into anesthetized non-tumor bearing Balb/c mice or HCT116 tumor bearing Balb/c nude mice; isofluorane/O_2/N_2O anesthesia was used. In a limited number of cases [^{11}C]choline (~9MBq) was used for comparison. Plasma samples were obtained at 2, 15, 30 and 60 min after injection; liver, kidney and tumor samples were obtained at 30 min. All samples were snap-frozen in liquid nitrogen. For analysis, samples were thawed and kept at 4°C immediately prior to use. To approximately 0.2 mL of plasma was added ice-cold methanol (1.5 mL). The mixture was then centrifuged (3 minutes, 15,493 × *g*; 4°C). The supernatant was evaporated to dryness using a rotary evaporator (Heidoloph Instruments GMBH & C0, Schwabach, Germany) at a bath temperature of 40°C. The residue was suspended in mobile phase (1.1 mL), clarified (0.2 μm filter) and analyzed by HPLC. Liver, kidney and tumor samples were homogenized in ice-cold methanol (1.5 mL) using an IKA Ultra-Turrax T-25 homogenizer and subsequently treated as per plasma samples. All samples were analyzed by radio-HPLC on an Agilent 1100 series HPLC system (Agilent Technologies, Stockport, UK) equipped with a γ-RAM Model 3 gamma-detector (IN/US Systems inc., Florida, USA) and Laura 3 software (Lablogic, Sheffield, UK). The stationary phase comprised of a Waters μBondapak C_{18} reverse-phase column (300 mm × 7.8 mm). Samples were analyzed using a mobile phase comprising of Solvent A (acetonitrile/water/ethanol/acetic acid/1.0 M ammonium acetate/0.1 M sodium phosphate) (800/127/68/2/3/10) and Solvent B (acetonitrile/water/ethanol/acetic acid/1.0 M ammonium acetate/0.1 M sodium phosphate) (400/400/68/44/88/10) with a gradient of 0% B for 6 min, then 0 → 100% B in 10 min, 100% B for 0.5 min, 100 → 0% B in 1.5 min then 0% B for 2 min, delivered at a flow rate of 3 ml/min. The analysis was based on that originally described by DeGrado and co-workers (17).

Metabolism of D4-FCH and FCH by HCT116 tumor cells

HCT116 cells were grown in T150 flasks in triplicate until they reached 70% confluent and then treated with vehicle (1% DMSO in growth media) or 1μM PD0325901 in vehicle for 24 h. Cells were pulsed for 1 hr with 1.1 MBq of D4-FCH or FCH. The cells were washed 3 times in ice cold PBS, scraped into 5 ml PBS and centrifuged at 500 × *g* for 3 min and then re-suspended in 2 ml of ice cold methanol for HPLC analysis as described above for tissue samples.

To provide biochemical evidence that the 5′ – phosphate, was the peak identified on the HPLC chromatogram, cultured cells were treated with alkaline phosphatase as described previously (32). Briefly, HCT116 cells were grown in 100mm dishes in triplicate and incubated with 5.0 MBq of FCH for 60 min at 37°C to form the putative FCH-phosphate. The cells were washed with 5 ml ice cold PBS twice and then scraped and centrifuged at 750 × *g* (4°C, 3 min) in 5 ml PBS. Cells were homogenized in 1 ml 5 mM Tris-HCl buffer

solution (pH 7.4) containing 50% (v/v) glycerol, 0.5 mM $MgCl_2$, and 0.5 mM $ZnCl_2$, and incubated with 10 units of bacterial (type III) alkaline phosphatase (Sigma) at 37°C in a shaking water bath for 30 min to dephosphorylate the FCH-phosphate. The reaction was terminated by adding ice cold methanol. Samples were processed as per plasma above and analyzed by radio-HPLC. Control experiments were performed without alkaline phosphatase.

Effect of PD0325901 treatment in mice

Size-matched HCT116 tumor-bearing mice were randomised to receive daily treatment by oral gavage of vehicle (0.5% hydroxypropyl methylcellulose plus 0.2% Tween 80) or 25mg/kg (0.005 ml/g mouse) of the mitogenic extracellular kinase inhibitor, PD0325901, prepared in vehicle. D4-FCH-PET scanning was performed after 10 daily treatments with the last dose administered 1 h before scanning. After imaging, tumors were snap-frozen in liquid nitrogen and stored at −80°C for analysis of choline kinase A (CHKA) expression.

PET imaging studies

Dynamic FCH and D4-FCH imaging scans were carried out on a dedicated small animal PET scanner, quad-HIDAC (Oxford Positron Systems, Weston-on-the-Green, United Kingdom). The features of this instrument have been described previously (32). For scanning the tail veins of vehicle- or drug-treated mice were cannulated after induction of anesthesia (isofluorane/O_2/N_2O). The animals were placed within a thermostatically controlled jig (calibrated to provide a rectal temperature of ~37°C) and positioned prone in the scanner. FCH or D4-FCH (2.96-3.7 MBq) was injected via the tail vein cannula and scanning commenced. Dynamic scans were acquired in list-mode format over a 60 min period as previously reported (33). The acquired data were sorted into 0.5-mm sinogram bins and 19 time frames (0.5 × 0.5 × 0.5 mm voxels; 4 × 15 s, 4 × 60 s, and 11 × 300 s) for image reconstruction, which was performed by filtered back-projection using a two-dimensional Hamming filter (cut-off 0.6). The image data-sets were visualized using the Analyze software (version 6.0; Biomedical Imaging Resource, Mayo Clinic, Rochester, MN).

Cumulative images of 30-60 min dynamic data were used for visualization of radiotracer uptake and to draw regions of interest (ROI). ROI were defined manually on five adjacent tumor regions (each 0.5 mm thickness). Dynamic data from these slices were averaged for each tissue (liver, kidney, muscle, urine and tumor) and at each of the 19 time points to obtain time versus radioactivity curves (TACs). Corresponding whole body TACs representing injected radioactivity were obtained by adding together radioactivity in all 200 × 160 × 160 reconstructed voxels. Tumor radioactivity was normalized to whole body radioactivity and expressed as percentage injected dose per voxel (%ID/vox). The normalized uptake of radiotracer at 60 min (%ID/vox_{60}) was used for subsequent comparisons. The average of the normalized maximum voxel intensity across five slices of tumor %IDvox_{60max} was also use for comparison to account for tumor heterogeneity and existence of necrotic regions in tumor. The area under the curve (AUC) was calculated as the integral of %ID/vox from 0-60 min.

Statistics

Statistical analyses were performed using the software GraphPad Prism, version 4 (GraphPad, San Diego, CA). Between-group comparisons were made using the nonparametric Mann-Whitney test. Two-tailed P value ≤ 0.05 were considered significant.

Results

D4-FCH is more resistant to oxidation *in vivo than FCH*

The relative rates of oxidation of the two isotopically radiolabeled choline species, FCH and D4-FCH (see structural formula in Fig. 1a) to their respective metabolites, FCH-betaine and D4-FCH-betaine was evaluated by high performance liquid chromatography (HPLC) in mouse plasma after intravenous injection of the radiotracers; the chromatographic method previously described by DeGrado and co-workers was used (17). As shown in Fig. 1b D4-FCH was markedly more stable to oxidation than FCH with ~40% conversion of D4-FCH to D4-FCH-betaine at 15 min after intravenous injection into mice compared to ~80% conversion of FCH to FCH-betaine. The time-course for *in vivo* oxidation is shown in Fig. 1c demonstrating overall improved stability of D4-FCH over FCH. Metabolite analysis of tissues including liver, kidney and tumor by HPLC was also accomplished. Typical HPLC chromatograms of FCH and D4-FCH and their respective metabolites in tissues are shown in Fig. S1. Choline and its metabolites lack any UV chromophore to permit presentation of chromatograms of the cold unlabelled compound simultaneously with the radioactivity chromatograms. Thus, we validated the presence of metabolites by other (chemical and biological) means. Of note the same chromatographic conditions were used for characterization of the metabolites and retention times were similar. We confirmed the identity of the phosphocholine peak biochemically by incubation of the putative phosphocholine formed in untreated HCT116 tumor cells with alkaline phosphatase Fig. S2. Chemical (potassium permanganate) and enzymatic (choline oxidase) methods were used to confirm the identity of the betaine peak (23) (data not shown). A high proportion of liver radioactivity was present as phosphocholine at 30 min post injection for both FCH and D4-FCH (Fig. 2a). An unknown metabolite (possibly the aldehyde intermediate) was observed in both the liver (7.4 ± 2.3%) and kidney (8.8 ± 0.2%) samples of D4-FCH treated mice. In contrast, this unknown metabolite was not found in liver samples of FCH treated mice and only to a smaller extent (3.3 ± 0.6%) in kidney samples. Notably 60.6 ± 3.7% of D4-FCH derived kidney radioactivity was phosphocholine compared to 31.8 ± 9.8% from FCH ($P = 0.03$). Conversely, most of the FCH-derived radioactivity in the kidney was in the form of FCH-betaine; 53.5 ± 5.3% compared to 20.6 ± 6.2% for D4-FCH (Fig. 2b). It could be argued that levels of betaine in plasma reflected levels in tissues such as liver and kidneys. Tumors showed a different HPLC profile compared to liver and kidneys; typical radio-HPLC chromatograms obtained from the analysis of tumor samples (30 min after intravenous injection of FCH, D4-FCH and [^{11}C]choline) are shown in Fig. S3. In tumors, radioactivity was mainly in the form of phosphocholine in the case of D4-FCH (Fig. 2c). In contrast, both FCH and [^{11}C]choline showed significant levels of FCH-betaine and [^{11}C]betaine. In the context of late imaging, these results indicate that D4-FCH will be the superior radiotracer for PET imaging with an uptake profile that is easier to interpret.

Tissue pharmacokinetics of FCH and D4-FCH by PET

FCH and D4-FCH were both rapidly taken up into tissues and retained (Fig. 3a and 3b). Tissue radioactivity increased in the order: muscle < urine < kidney < liver. Given the predominance of phosphorylation over oxidation in the liver (Fig. 2a), we found little differences in overall liver radioactivity levels between the two radiotracers. Liver radioactivity at levels 60 min after D4-FCH or FCH injection, %ID/vox$_{60}$, was 20.92 ± 4.24 and 18.75 ± 4.28, respectively (Fig. 3a and b). This is also in keeping with the lower levels betaine with D4-FCH injection than with FCH injection (Fig. 2a). Thus, pharmacokinetics of the two radiotracers in liver determined by PET (which lacks chemical resolution) were similar. The lower kidney radioactivity levels for D4-FCH compared to FCH (Fig. 3a and b), on the other hand, reflect the lower oxidation potential of D4-FCH in kidneys (Fig 2b). The %ID/vox$_{60}$ for FCH and D4-FCH were 15.97 ± 4.65 and 7.59 ± 3.91, respectively in

kidneys (Fig. 3a and b). Urinary excretion was similar between the radiotracers. ROIs that were drawn over the bladder showed %ID/vox$_{60}$ values of 5.20 ± 1.71 and 6.70 ± 0.71 for D4-FCH and FCH, respectively. Urinary metabolites comprised mainly of the unmetabolized radiotracers (data not shown). Muscle showed the lowest radiotracer levels of any tissue.

D4-FCH shows higher sensitivity for imaging tumors by PET

Given the relatively high systemic stability of D4-FCH and high proportion of phosphocholine metabolites, it was reassuring to observe higher tumor radiotracer uptake by PET in mice that were injected with D4-FCH compared to the FCH group. Fig. 4a shows typical (0.5 mm) transverse PET image slices demonstrating accumulation of FCH and D4-FCH in human melanoma SKMEL-28 xenografts. In this mouse model, the tumor signal-to-background contrast was qualitatively superior in the D4-FCH PET images compared to FCH images. Both radiotracers had similar tumor kinetic profiles detected by PET (Fig. 4b). The kinetics were characterized by rapid tumor influx with peak radioactivity at ~1 min (Fig. 4b). Tumor levels then equilibrated until ~5 min followed by a plateau. The delivery and retention of D4-FCH were quantitatively higher than those for FCH (Fig. 4c). The %ID/vox$_{60}$ for D4-FCH and FCH were 7.43 ± 0.47 and 5.50 ± 0.49, respectively (P=0.04). Because tumors often present with heterogeneous population of cells, we exploited another imaging variable that is probably less sensitive to experimental noise – an average of the maximum pixel %ID/vox$_{60}$ across 5 slices (%IDvox$_{60max}$). This variable was also significantly higher for D4-FCH (P=0.05; Fig. 4c). Furthermore, tumor area under the time versus radioactivity curve (AUC) was higher for D4-FCH mice than FCH (P =0.02). Although the 30 min time point was selected for a more detailed analysis of tissue samples, it should be noted that the percentage of parent compound in plasma was consistently higher for D4-FCH compared to FCH at earlier time points. Regarding imaging, tumor uptake for both radiotracers was similar at the early (15 min) and late (60 min) time points (Supplementary Table1). The earlier time points may be appropriate for pelvic imaging.

D4-FCH detects response to treatment

Having demonstrated that D4-FCH was a more stable fluorinated-choline analog for *in vivo* studies, we wanted to investigate if this radiotracer could be used to measure response to therapy. We chose to perform these studies in a reproducible tumor model system in which treatment outcomes have been previously characterized, i.e., the human colon carcinoma xenograft HCT116 treated with PD0325901 daily for 10 days (31). Drug treatment led to tumor stasis (reduction in tumor size by only 12.2% at day 10 compared to the pretreatment group); tumors of vehicle-treated mice increased by 375%. Tumor D4-FCH levels in PD0325901-treated mice peaked at approximately the same time as those of vehicle-treated ones, however, there was a marked reduction in radiotracer retention in the treated tumors (Fig. 5a). All imaging variables decreased after 10 days of drug treatment (P=0.05, Fig. 5b). This indicates that D4-FCH can be used to detect treatment response even under conditions where large changes in tumor size reduction are not seen (31). To understand the biomarker changes, we examined the intrinsic cellular effect of PD0325901 on D4-FCH-phosphocholine formation by treating exponentially growing HCT116 cells in culture with PD0325901 for 24 h and measuring the 60-min uptake of D4-FCH *in vitro*. As shown in Fig. 5c., PD0325901 significantly inhibited D4-FCH-phosphocholine formation in drug-treated cells demonstrating that the effect of the drug in tumors is likely due to cellular effects on choline metabolism rather than hemodynamic effects.

To understand further the mechanisms regulating D4-FCH uptake with drug treatment, we assessed changes in CHKA expression in PD0325901- and vehicle-treated tumors excised after PET scanning. A significant reduction in CHKA protein expression was seen *in vivo* at

day 10 (P=0.03) following PD0325901 treatment (Fig. 6) indicating that reduced CHKA expression contributed to the lower D4-FCH uptake in drug-treated tumors. The drug-induced reduction of CHKA expression also occurred *in vitro* in exponentially growing cells treated with PD0325901 (data not shown).

Discussion

We have designed, synthesized and established utility of a novel radiolabeled choline analog for tumor imaging. Many cancers have elevated phospholipid biosynthesis to meet the demand of rapid tumor cell growth, and in these cancers, phosphocholine serves as an important mediator of transmembrane signaling (34, 35). Choline is taken into cells by a specific transport mechanism and phosphorylated by choline kinase which is constitutively active in many cancer cells (10, 36, 37). This metabolic process serves to trap choline in cells as phosphocholine, thus, radiolabeled analogs of choline are being explored as radiotracers for imaging tumors by PET. FCH, originally developed by De Grado and co-workers, is currently been evaluated for imaging prostate cancer, and other malignancies (17, 22, 38, 39). In this study, we report the development of a more stable FCH analog, D4-FCH, for cancer detection in which substitution of deuterium for hydrogen on the ethyl alcohol portion of choline results in a large observed isotope effect in the oxidation of choline to betaine by choline oxidase (25-27). Kinetic studies indicate that the magnitude of the $^{1}H/^{2}D$ isotope effect is the result of environmentally enhanced quantum tunneling involving a highly pre-organized enzyme active site, where the probability of tunneling decreases with the increased mass of deuterium in a molecule (24). The biological effect of this substitution is to reduce oxidation and increase the net availability of the parent tracer for phosphorylation and trapping within cells leading to improved signal-to-background contrast for PET imaging of tumors *in vivo* (40-42)

Improved stability of D4-FCH over FCH for late imaging after clearance was supported initially (0-30 min) by the higher proportion of parent radiotracer in plasma, but this difference appeared to have been lost by 60 min when the parent radiotracers had been completely metabolized (Fig. 1c). We interpret this finding as a model limitation: the capacity of rodents to metabolize choline analogs (43) is substantially higher than that of humans (23) and so we expect the early differential between the two radiotracers to be maintained in humans. Improved stability of D4-FCH over FCH was demonstrated as reduced levels of D4-FCH oxidation products in plasma of mice injected intravenously with the radiotracers. The oxidation product of D4-FCH was also lower in at least one of two major organs responsible for choline oxidation/choline oxidase activity - liver and kidney (23, 39, 43). The reduced oxidation of D4-FCH resulted, for instance, in a 2-fold lower total radioactivity level in kidney. Tissue HPLC analysis also confirmed that most of the D4-FCH was trapped specifically in the form of phosphocholine whereas betaine was the main metabolite from FCH in kidneys. It is possible that kidneys have a lower capacity for phosphorylating the free D4-FCH. In liver, on the other hand, unmetabolized FCH and D4-FCH were rapidly phosphorylated and the predominance of phosphorylation may explain the similar levels of liver radioactivity for both radiotracers. Notably, betaine levels in liver were higher for FCH than D4-FCH. Betaine, like phosphocholine, is a charged molecule and is also expected to be trapped in cells to a reasonable extent; unlike phosphocholine, however, it is exported into circulation as shown in this study.

One advantage of using radiolabeled choline analogs for pelvic imaging is their low renal elimination. Urine levels of choline analogs result largely from unmetabolized parent radiotracer (data not shown) as betaine analogs are efficiently reabsorbed in the kidney tubules (44, 45). Due to their ionization properties, oxidation intermediates (such as aldehyde) are unlikely to be re-absorbed efficiently within the kidney tubules and could

contribute to urinary radioactivity (45). It was a concern that the high stability of D4-FCH, and hence higher levels of parent radiotracer in plasma will lead to high levels of radioactivity in the urine. Compared to [^{11}C]choline, FCH was found to have less desirable urinary excretion properties. We have not been able to demonstrate that D4-FCH used under the same conditions will overcome this limitation. It may be possible, however, for patients to void urine at late time points to reduce bladder radioactivity.

Of interest, both FCH and [^{11}C]choline showed high levels of betaine metabolites in tumor, whereas very little betaine metabolite was found following D4-FCH injection. The improved stability of D4-FCH will permit late imaging to be performed with confidence since metabolism will be less of a concern. In a late imaging protocol, voiding can further reduce the spill-over contribution of bladder radioactivity. Improved stability of D4-FCH also led to increased tumor radioactivity by 1.3-fold compared to FCH. This increased tumor retention could be ascribed to increased availability of substrate for phosphorylation and reduced competing (oxidation) reactions that leads to betaine formation and elimination of the latter. Having demonstrated superior pharmacokinetics, we further established utility of D4-FCH for response monitoring. D4-FCH was found to be a useful radiotracer for monitoring the effect of MEK inhibition by PD0325901 in a model where the drug effects are largely cytostatic at the dose used. The reduction in radiotracer uptake following drug treatment *in vivo* was intrinsic to changes in cellular biochemistry as demonstrated *in vitro* and could be ascribed at least in part to reduced CHKA expression.

In translating our findings into clinical imaging, it should be noted that oxidation of choline is faster in rodents (38) compared to humans (23). Thus, we expect the rate of D4-FCH oxidation to be even lower in humans; this may lead to further improvements in detection sensitivity in humans consequent to the higher overall levels of phosphorylated D4-FCH. In conclusion, we have demonstrated that the novel radiotracer, D4-FCH, has improved stability and sensitivity for detection of choline metabolism *in vivo*. The radiotracer also has potential for detecting response to anti-cancer drug treatment. These promising attributes warrant further pre-clinical and clinical development of D4-FCH.

Supplementary Material

Refer to Web version on PubMed Central for supplementary material.

Acknowledgments

Funding support from Cancer Research UK & Engineering & Physical Sciences Research Council (C2536/A10337), and the UK Medical Research Council (U1200.005.00001.01).

The abbreviations used include the following

FCH	[^{18}F]fluorocholine
D4-FCH	[^{18}F]fluoromethyl-[1,2-$^{2}H_4$]-choline
PET	positron emission tomography
s.c.	subcutaneous
i.v.	intravenous
PBS	phosphate buffered saline
CHKA	choline kinase type A
TAC	time versus radioactivity curve

ROI	region of interest
%ID/vox$_{60}$	% injected dose per voxel
%ID/vox$_{max}$	maximal % injected dose per voxel
AUC	area under the time versus radioactivity curve
MEK1/2	mitogenic extracellular kinase 1/2

REFERENCES

1. Aboagye EO, Bhujwalla ZM. Malignant transformation alters membrane choline phospholipids metabolism of human mammary epithelial cell. Cancer Res. 1999; 59:80–4. [PubMed: 9892190]
2. Exton JH. Phosphatidylcholine breakdown and signal transduction. Biochim Biophys Acta. 1994; 1212:26–42. [PubMed: 8155724]
3. George TP, Morash SC, Cook HW, Byers DM, Palmer FBSC, Spence MW. Phosphatidylcholine biosynthesis in cultured glioma cells: evidence for channelling of intermediates. Biochim Biophys Acta. 1989; 104:283–91. [PubMed: 2758024]
4. Teegarden D, Taparowsky EJ, Kent C. Altered phosphatidylcholine metabolism in C3H10T1/2 cells transfected with the Harvey-ras oncogene. J Biol Chem. 1990; 265:6042–7. [PubMed: 2156839]
5. Aoyama C, Liao H, Ishidate K. Structure and function of choline kinase isoforms in mammalian cells. Prog Lipid Res. 2004; 43:266–81. [PubMed: 15003397]
6. Glunde K, Jie C, Bhujwalla ZM. Molecular causes of the aberrant choline phospholipid metabolism in breast cancer. Cancer Res. 2004; 64:4270–6. [PubMed: 15205341]
7. Glunde K, Raman V, Mori N, Bhujwalla ZM. RNA interference-mediated choline kinase suppression in breast cancer cells induces differentiation and reduces proliferation. Cancer Res. 2005; 65:11034–43. [PubMed: 16322253]
8. Iorio E, Mezzanzanica D, Alberti P, et al. Alterations of choline phospholipid metabolism in ovarian tumor progression. Cancer Res. 2005; 65:9369–76. [PubMed: 16230400]
9. Ramirez de Molina A, Rodriguez-Gonzalez A, Gutierrez R, et al. Overexpression of choline kinase is a frequent feature in human tumor-derived cell lines and in lung, prostate, and colorectal human cancers. Biochem Biophys Res Commun. 2002; 296:580–3. [PubMed: 12176020]
10. Ramirez de Molina A, Sarmentero-Estrada J, Belda-Iniesta C, et al. Expression of choline kinase alpha to predict outcome in patients with early-stage non-small-cell lung cancer: a retrospective study. Lancet Oncol. 2007; 8:889–97. [PubMed: 17851129]
11. Hara T, Inagaki K, Kosaka N, Morita T. Sensitive detection of mediastinal lymphnode metastasis of lung cancer with [11C]-choline PET. J Nucl Med. 2000; 41:1507–13. [PubMed: 10994730]
12. Hara T, Kosaka N, Kishi H. PET imaging of prostate cancer using carbon-11-choline. J Nucl Med. 1998; 39:990–5. [PubMed: 9627331]
13. Hara T, Kosaka N, Shinoura N, Kondo T. PET imaging of brain tumor with [methyl-11C]choline. J Nucl Med. 1997; 38:842–7. [PubMed: 9189127]
14. Kobori O, Kirihara Y, Kosaka N, Hara T. Positron emission tomography of esophageal carcinoma using [11C]-choline and 18F-fluorodeoxyglucose. Cancer Cell. 1999; 86:1638–48.
15. Pieterman RM, Que TH, Elsinga PH, et al. Comparison of [11C]-choline and [18F]-FDG PET in primary diagnosis and staging of patients with thoracic cancer. J Nucl Med. 2002; 43:167–72. [PubMed: 11850480]
16. Reske SN. 11C-Choline uptake with PET/CT for the initial diagnosis of prostate cancer: relation to PSA levels, tumour stage and anti-androgenic therapy. Eur J Nucl Med Mol Imaging. 2008; 35:1741.
17. DeGrado TR, Coleman RE, Wang S, et al. Synthesis and evaluation of [18F]-labeled choline as an oncologic tracer for positron emission tomography: initial findings in prostate cancer. Cancer Res. 2001; 61:110–7. [PubMed: 11196147]

18. Beheshti M, Vali R, Waldenberger P, et al. Detection of bone metastases in patients with prostate cancer by 18F fluorocholine and [18F]-fluoride PET-CT: a comparative study. Eur J Nucl Med Mol Imaging. 2008; 35:1766–74. [PubMed: 18465129]
19. Cimitan M, Bortolus R, Morassut S, et al. [18F]-fluorocholine PET/CT imaging for the detection of recurrent prostate cancer at PSA relapse: experience in 100 consecutive patients. Eur J Nucl Med Mol Imaging. 2006; 33:1387–98. [PubMed: 16865395]
20. de Jong IJ, Pruim J, Elsinga PH, Jongen MM, Mensink HJ, Vaalburg W. Visualization of bladder cancer using 11Ccholine PET: first clinical experience. Eur J Nucl Med Mol Imaging. 2002; 29:1283–8. [PubMed: 12271408]
21. Price DT, Coleman RE, Liao RP, Robertson CN, Polascik TJ, DeGrado TR. Comparison of [18F]fluorocholine and [18F]fluorodeoxyglucose for positron emission tomography of androgen dependent and androgen independent prostate cancer. J Urol. 2002; 168:273–80. [PubMed: 12050555]
22. DeGrado TR, Reiman RE, Price DT, Wang S, Coleman RE. Pharmacokinetics and radiation dosimetry of [18F]-fluorocholine. J Nucl Med. 2002; 43:92–6. [PubMed: 11801711]
23. Roivainen A, Forsback S, Gronroos T, et al. Blood metabolism of [methyl-11C]choline; implications for in vivo imaging with positron emission tomography. Eur J Nucl Med. 2000; 27:25–32. [PubMed: 10654143]
24. Fan F, Gadda G. An internal equilibrium preorganizes the enzyme-substrate complex for hydride tunneling in choline oxidase. Biochemistry. 2007; 46:6402–8. [PubMed: 17472346]
25. Fan F, Gadda G. On the catalytic mechanism of choline oxidase. J Am Chem Soc. 2005; 127:2067–74. [PubMed: 15713082]
26. Gadda G. pH and deuterium kinetic isotope effects studies on the oxidation of choline to betaine-aldehyde catalyzed by choline oxidase. Biochimica et Biophysica Act. 2003; 1650:4–9.
27. Nagel ZD, Klinmn JP. Tunneling and dynamics in enzymatic hydride transfer. Chem Rev. 2006; 106:3095–118. [PubMed: 16895320]
28. Bergman J, Eskola O, Lehikoinen P, Solin O. Automated synthesis and purification of [18F]bromofluoromethane at high specific radioactivity. Applied Radiation and Isotopes. 2001; 54:927–33. [PubMed: 11300406]
29. Pascali C, Itawa R, Cambiè M, Bombardieri E. [11C]-Methylation on a C18 Sep-Pak cartridge: a convenient way to produce [N-methyl-11C]choline. J Labelled Compds Radiopharm. 2000; 43:195–203.
30. Workman P, Balmain A, Hickman JA, et al. UKCCCR guidelines for the welfare of animals in experimental neoplasia. Lab Anim. 1988; 22:195–201. [PubMed: 3172698]
31. Leyton J, Smith G, Lees M, et al. Noninvasive imaging of cell proliferation following mitogenic extracellular kinase inhibition by PD0325901. Mol Cancer Ther. 2008; 7:3112–21. [PubMed: 18790789]
32. Barthel H, Cleij MC, Collingridge DR, et al. 3′-Deoxy-3′-[18F]Fluorothymidine as a new marker for monitoring tumor response to antiproliferative therapy in vivo with positron emission tomography. Cancer Research 63. 2003; 63:3791–8.
33. Leyton J, Alao JP, Da Costa M, et al. In vivo Biological Activity of the Histone Deacetylase Inhibitor LAQ824 Is detectable with 3′-Deoxy-3′-[18F]Fluorothymidine Positron Emission Tomography. Cancer Res. 2006; 66:7621–9. [PubMed: 16885362]
34. Zeisel SH. Choline phospholipids: signal transduction and carcinogenesis. FASEB J. 1993; 7:551–7. [PubMed: 8472893]
35. Zeisel SH. Nutrients, signal transduction and carcinogenesis. Adv Exp Med Biol. 1995; 369:175–83. [PubMed: 7598005]
36. Katz-Brull R, Degani H. Kinetics of choline transport and phosphorylation in human breast cancer cells; NMR application of the zero trans method. Anticancer Res. 1996; 16:1375–80. [PubMed: 8694504]
37. Katz-Brull R, Seger D, Rivenson-Segal D, Rushkin E, Degani H. Metabolic markers of breast cancer: enhanced choline metabolism and reduced choline-ether-phospholipid synthesis. Cancer Res. 2002; 62:1966–70. [PubMed: 11929812]

38. Bensal A, Shuyan W, Hara T, Harris RA, Timothy R, DeGrado TR. Biodisposition and metabolism of [18F]fluorocholine in 9L glioma cells and 9L glioma-bearing fisher rats. Eur J Nucl Med Mol Imaging. 2008; 35:1192–203. [PubMed: 18264706]
39. Kwee SA, DeGrado TR, Talbot JN, Gutman F, Coel MN. Cancer imaging with fluorine-18-labeled choline derivatives. Semin Nucl Med. 2007; 37:420–8. [PubMed: 17920349]
40. Fowler JS, Wolf AP, MacGregor RR, et al. Mechanistic positron emission tomography studies: demonstration of a deuterium isotope effect in the monoamine oxidase-catalyzed binding of [11C]L-deprenyl in living baboon brain. J Neurochem. 1988; 51:1524–34. [PubMed: 3139834]
41. Schou M, Halldin C, Sovago J, et al. PET evaluation of novel radiofluorinated reboxetine analogs as norepinephrine transporter probes in the monkey brain. Synapse. 2004; 53:57–67. [PubMed: 15170818]
42. van Dyck CH, Soares JC, Tan PZ, et al. Equilibrium modeling of 5-HT(2A) receptors with [18F]-deuteroaltanserin and PET: feasibility of a constant infusion paradigm. Nucl Med Biol. 2000; 27:715–22. [PubMed: 11150702]
43. Haubrich DR, Wang PF, Wedeking PW. Distribution and metabolism of intravenously administered choline[methyl- 3-H] and synthesis in vivo of acetylcholine in various tissues of guinea pigs. J Pharmacol. 1975; 193:246–55.
44. Lever M, Sizeland PC, Bason LM, Hayman CM, Chambers ST. Glycine betaine and proline betaine in human blood and urine. Biochim Biophys Acta. 1994; 1200:259–64. [PubMed: 8068711]
45. Pummer S, Dantzler WH, Lien YH, Moeckel GW, Volker K, Silbernagl S. Reabsorption of betaine in Henle's loops of rat kidney in vivo. Am J Physiol Renal Physiol. 2000; 278:F434–9. [PubMed: 10710548]

Europe PMC Funders Author Manuscripts

Europe PMC Funders Author Manuscripts

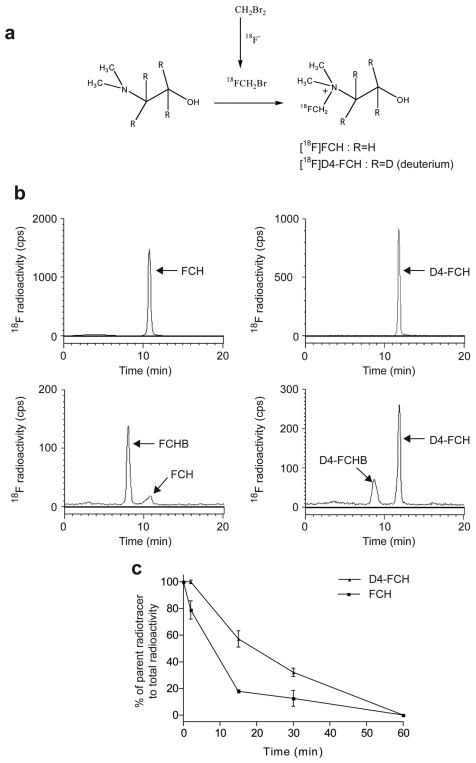

Figure 1.

Synthesis of D4-FCH. (**a**) No-carrier-added D4-FCH was synthesized by reacting [^{18}F]fluorobromomethane with N,N-dimethylaminoethanol or d4-N,N-dimethylaminoethanol. (**b)** Analysis of the metabolism of FCH to FCH-betaine and D4-FCH to D4-FCH-betaine by radio-HPLC in mouse plasma samples obtained 15 min after injecting the tracers intravenously into mice (**c)** A summary of the conversion of parent tracers, FCH and D4-FCH, to metabolites, FCH-betaine (FCHB) and D4-FCH betaine (D4-FCHB), in plasma. Data are mean (± SE); n=3 mice.

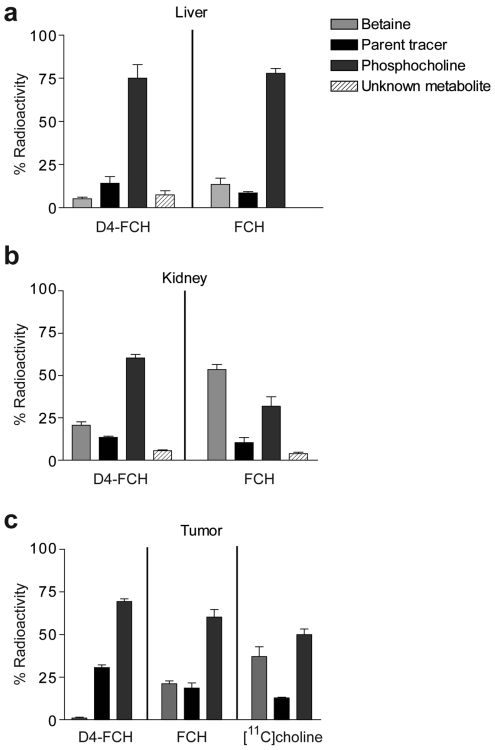

Figure 2.

Metabolite profile in mouse tissues after intravenous injection of parent radiotracers, FCH and D4-FCH, assessed by radio-HPLC. The % radioactivity remaining at 30 min in the form of parent radiotracer, phosphocholine or betaine analogs, as well as that of unknown metabolites are shown for **(a)** liver, (**b)** kidney and **(c)** HCT116 tumor. In the case of tumor, additional comparisons were done with [^{11}C]choline.

Europe PMC Funders Author Manuscripts

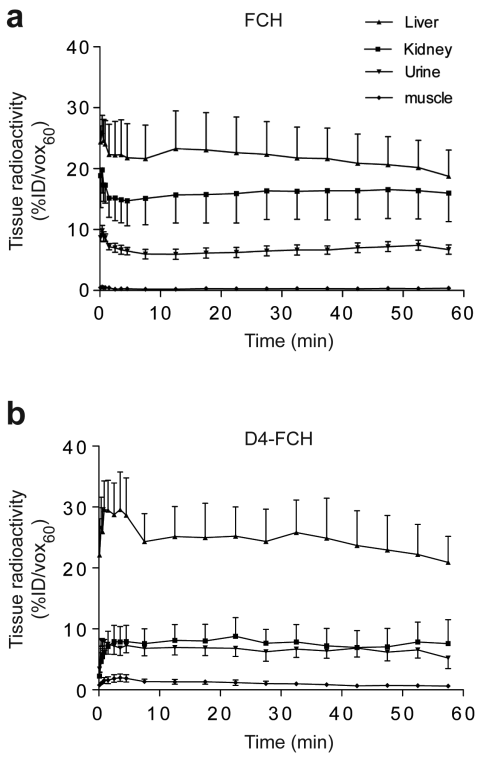

Figure. 3.

Tissue profile of FCH and D4-FCH. **(a)** Time versus radioactivity curve for the uptake of FCH in liver, kidney, urine (bladder) and muscle derived from PET data, and (**b)** corresponding data for D4-FCH. Results are the mean ± SE; n = 4 mice. For clarity upper and lower error bars (SE) have been used.

Europe PMC Funders Author Manuscripts

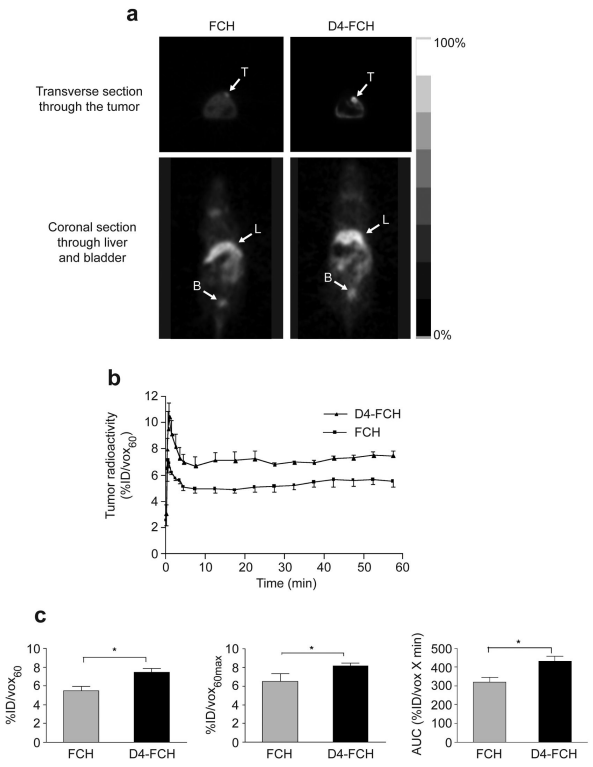

Figure 4.

Tumor profile of FCH and D4-FCH in SKMEL28 tumor xenograft. **(a)** Typical FCH-PET and D4-FCH-PET images of SKMEL28 tumor-bearing mice showing 0.5 mm transverse sections through the tumor and coronal sections through the bladder. For visualization, 30 to 60 min summed image data are displayed. Arrows point to the tumors (T), liver (L) and bladder (B). (**b).** Comparison of time versus radioactivity curves for FCH and D4-FCH in tumors. For each tumor, radioactivity at each of 19 time frames was determined. Data are mean $\%ID/vox_{60}$ mean ± SE (n = 4 mice per group). (**c)** Summary of imaging variables. Data are mean ± SE, n = 4; *P = 0.04. For clarity upper and lower error bars (SE) have been used.

Europe PMC Funders Author Manuscripts

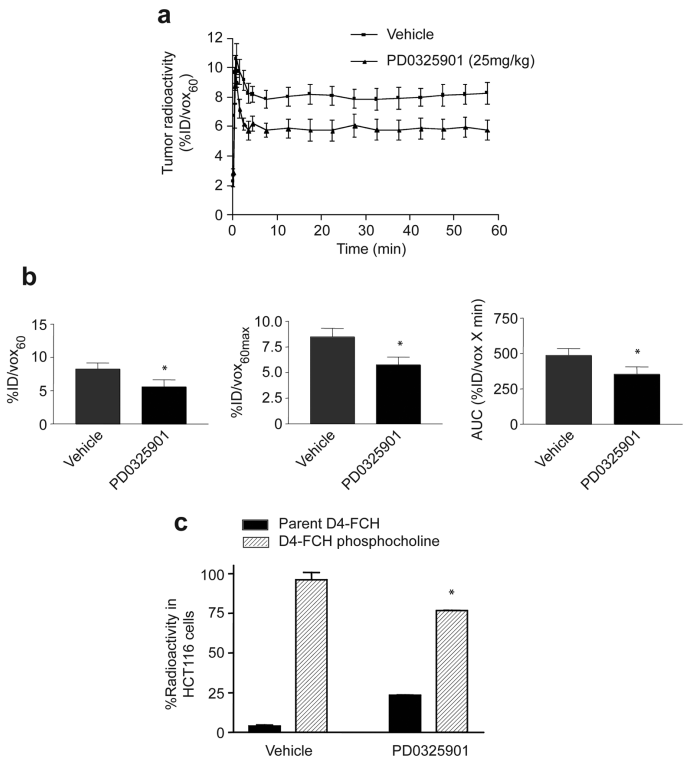

Figure 5.

Effect of PD0325901 on uptake of D4-FCH in HCT116 tumors and cells. (**a)** Normalized time versus radioactivity curves in HCT116 tumors following daily treatment for 10 days with vehicle or 25mg/kg PD0325901. Data are the mean ± SE; n = 3 mice. (**b)** Summary of imaging variables $\%ID/vox_{60}$, $\%ID/vox_{60max}$, and AUC. Data are mean ± SE; * P = 0.05. **(c)** Intrinsic cellular effect of PD0325901 (1μM) on D4-FCH phosphocholine metabolism after treating HCT116 cells for 1 hr with D4-FCH in culture. Data are mean ± SE; n=3 ; * P = 0.03.

Europe PMC Funders Author Manuscripts

Europe PMC Funders Author Manuscripts

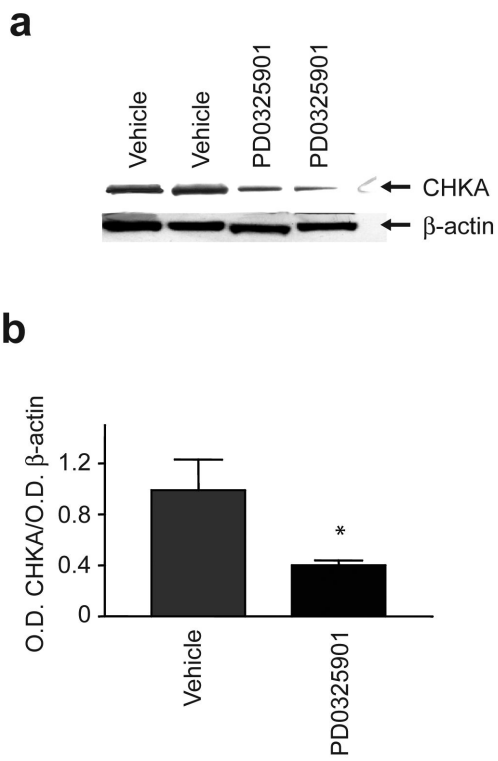

Figure 6.

Expression of choline kinase A in HCT116 tumors. **(a)** A typical Western blot demonstrating the effect of PD0325901 on tumor choline kinase A (CHKA) protein expression. HCT116 tumors from mice that were injected with PD0325901 (25mg/kg daily for 10 days, orally) or vehicle were analyzed for CHKA expression by western blotting. β-actin was used as the loading control. **(b)** Summary densitometer measurements for CHKA expression expressed as a ratio to β-actin. The results are the mean ratios ± SE; n = 3, * P = 0.05.